Supplementary Material

Supplementary Table S1: Oligonucleotides used for the generation of the *Xcc*FimX^{EAL} and *Xcc*PilZ$_{1028}$ variants.

	Oligonucleotides	Sequences (5'-3')
*Xcc*FimX^{EAL}	EAL-Q40A (f)	GCTGGAGCTGTATGCGGCGTTCCTGCG
	EAL-Q40A (r)	CGCAGGAACGCCGCATACAGCTCCAGC
	EAL-F42A (f)	CTGTATCAGGCGGCCCTGCGGCTGGAG
	EAL-F42A (r)	CTCCAGCCGCAGGGCCGCCTGATACAG
	EAL-S53A (f)	TGGCGAGATGATGGCGCCGAATGCG
	EAL-S53A (r)	CGCATTCGGCGCCATCATCTCGCCA
	EAL-R97A (f)	CACCTGCTGGTGGCCATCGGGCCCAA
	EAL-R97A (r)	TTGGGCCCGATGGCCACCAGCAGGTG
	EAL-E159A (f)	AGGTGGGGCTGGCGCAATTCGGTTC
	EAL-E159A (r)	GAACCGAATTGCGCCAGCCCCACCT
	EAL-E216A (f)	TCACGGTGGCCGCGTTCGTGGCCGA
	EAL-E216A (r)	TCGGCCACGAACGCGGCCACCGTGA
	EAL-F217A (f)	ACGGTGGCCGAGGCCGTGGCCGATGC
	EAL-F217A (r)	GCATCGGCCACGGCCTCGGCCACCGT
*Xcc*PilZ$_{1028}$	PilZ-K30A (f)	CCGTTCGTGGCAAGTGGCGGCATCTTCGTG
	PilZ-K30A (r)	CCGCCACTTGCCACGAACGGCATGTAGGCG
	PilZ-G45A (f)	CGCTACATGCTGGCCGATGAGGTGTTTCTG
	PilZ-G45A (r)	CAGAAACACCTCATCGGCCAGCATGTAGCG
	PilZ-G45V (f)	CGCTACATGCTGGTCGATGAGGTGTTTCTG
	PilZ-G45V (r)	CAGAAACACCTCATCGACCAGCATGTAGCG
	PilZ-K66A (f)	TCCCGGTCGCCGGCGCGGTGGTGTGGACCA
	PilZ-K66A (r)	TGGTCCACACCACCGCGCCGGCGACCGGGA

Supplementary Table S2: Interaction distances in the binary *Xcc*FimX^{EAL}–c-di-GMP and ternary *Xcc*FimX^{EAL}–c-di-GMP–*Xcc*PilZ$_{1028}$ complexes

*Xcc*FimX^{EAL}		c-di-GMP		*Xcc*PilZ$_{1028}$
D^{71}-O$^{\delta1}$	**(2.51)¶, 4.47**	**Gua1-N^{1}**		
D^{71}-O$^{\delta1}$	**(2.24), 4.70**	**Gua1-N^{2}**		
L^{43}-N	**(3.33), > 5.0**	**Gua1-O^{6}**		
L^{43}-N	**(2.96), 4.41**	**Gua1-N^{7}**		
S^{53}-O$^{\gamma}$	(2.60), 3.15	P^{1}-O^{1}		
R^{44}-N^{H1}	(2.77), 2.07	P^{1}-O^{1}		
R^{44}-N^{H2}	(3.52), 1.92	P^{1}-O^{2}		
R^{44}-N^{H1}	(2.31), 2.65	P^{1}-O^{2}		
R^{44}-N^{H2}	(3.70), 3.42	P^{1}-O^{1}		
R^{44}-N^{H2}	(3.97), 3.96	Gua2-O2’		
T^{243}- O$^{\gamma}$	(3.40), > 5.0	Gua2-O2’		
D^{238}-O$^{\delta1}$	**(2.27), > 5.0**	**Gua2-N^{7}**		
D^{238}-O$^{\delta1}$	**(> 5.0), 2.09**	**Gua2-N^{1}**		
D^{238}-O$^{\delta1}$	**(> 5.0), 2.35**	**Gua2-N^{2}**		
F^{217}-N	**(2.61), > 5.0**	**Gua2-O^{6}**		
E^{216}-O$^{\varepsilon1}$	**(2.05), > 10.0**	**Gua2-N^{1}**		
E^{216}-O$^{\varepsilon1}$	**(2.29), > 10.0**	**Gua2-N^{2}**		
R^{97}-N^{H1}	(1.90), 2.23	P^{2}-O^{1}		
R^{183}-N^{H1}	(> 7.0)^{ǂ}, 3.99	**Gua2-N^{2}**		
R^{183}-N^{H2}	(> 7.0)^{ǂ}, 4.58	**Gua2-N^{2}**		
		Gua1-O2’	2.27	K^{30}-N$^{\zeta}$
		P^{2}-O^{2}	2.19	K^{66}-N$^{\zeta}$
		Gua2-O2’	2.01	G^{45}-N
		Gua2-N^{3}	1.93	G^{45}-O
		Gua2-N^{2}	2.99	G^{45}-O

The values in parenthesis are interaction distances between *Xcc*FimX^{EAL} and c-di-GMP while those in the right are between *Xcc*FimX^{EAL}–*Xcc*PilZ$_{1028}$ complex and c-di-GMP. C-di-GMP Gua1 and Gua2 interactions exhibit the most difference between the two complexes and were listed in bold.

ǂ The phenyl ring of F^{217} sandwiches between the Gua2 base and guanido group of R^{183}.

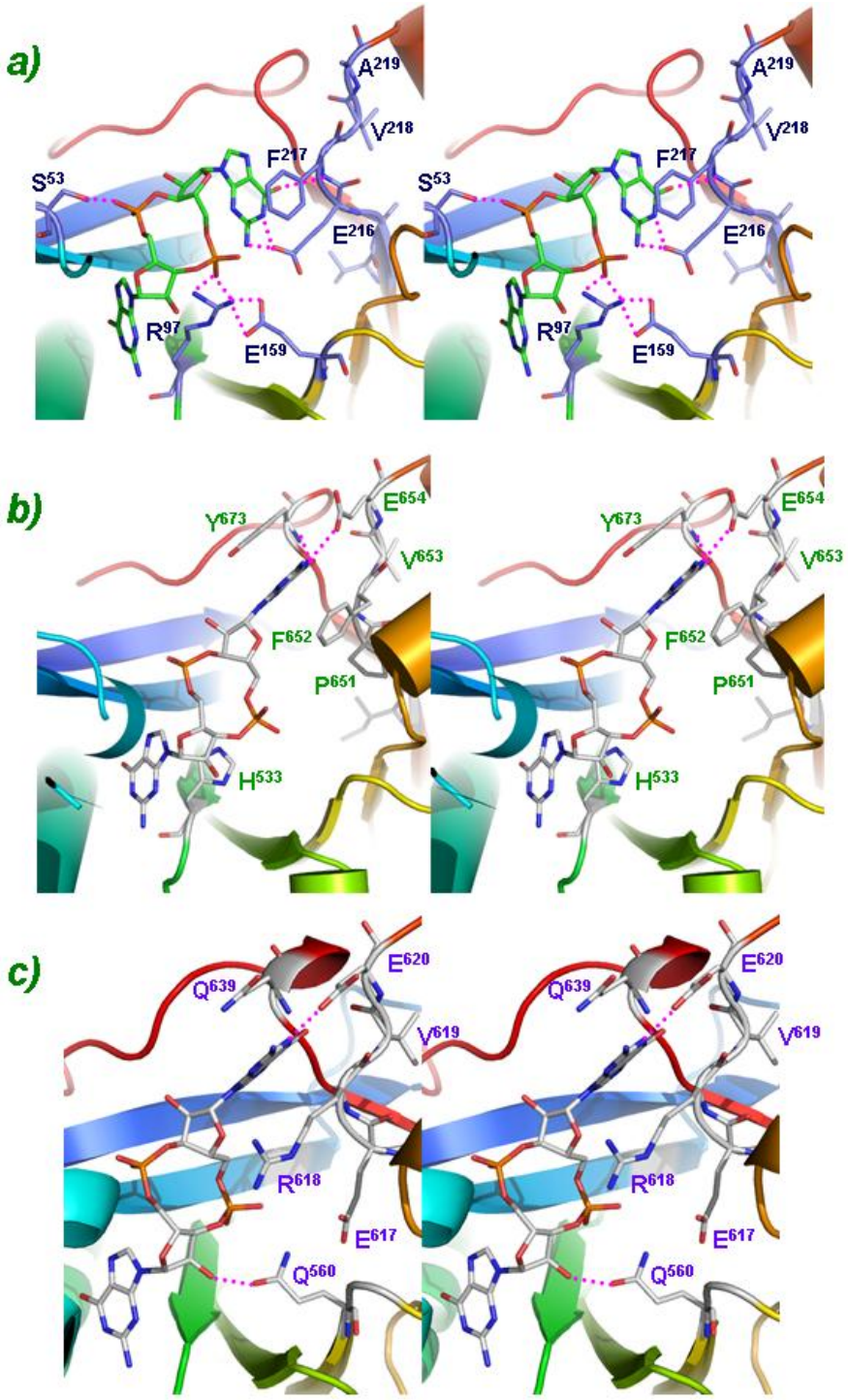

Supplementary Figure S1. Comparison among the c-di-GMP binding sites of the *Xcc*FimX^{EAL}, and *Pa*FimX^{EAL}, and *Pf*LapD^{EAL} domains. This figure reveals the dramatically different conformation of c-di-GMP in the *Xcc*FimX^{EAL}–c-di-GMP binary complex, compared to other degenerate EAL domain proteins, possibly due to the different tetra-residue motifs surrounding the binding sites.

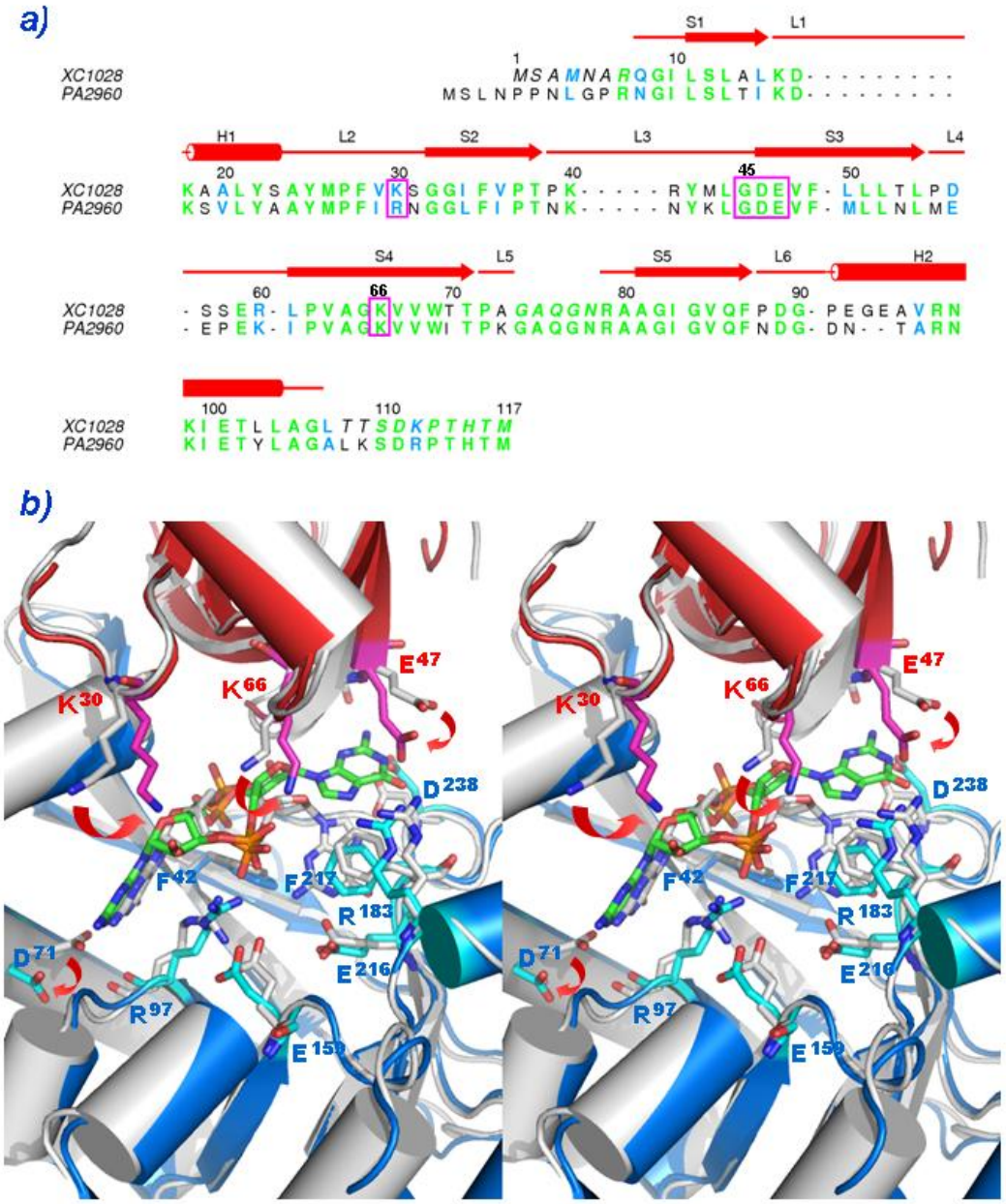

Supplementary Figure S2. a) Sequence alignments of the type II *Xcc*PilZ$_{1028}$ and PA2960. The residues important in recognizing c-di-GMP and *Xcc*FimX^{EAL} domain (boxed in red) seem to be conserved between the two sequences. b) Stereo diagram of superimposition between the *Xcc*FimX^{EAL}–c-di-GMP–*Xcc*PilZ$_{1028}$ ternary complex and the *Xcc*FimX^{EAL}–c-di-GMP binary complex and the *Xcc*PilZ$_{1028}$ monomer. The *Xcc*FimX^{EAL} domain and the *Xcc*PilZ$_{1028}$ domain in the ternary complex were drawn in blue cartoon and red cartoon, while the *Xcc*FimX^{EAL} domain in the binary complex

and that of the isolated *Xcc*PilZ$_{1028}$ domain were drawn in gray cartoon. The side chains of K^{30}, K^{66}, and E^{47} adopt different rotamers to better interact with the c-di-GMP and the *Xcc*FimX^{EAL} domain, but the global conformation of the *Xcc*PilZ$_{1028}$ domain does not change much.

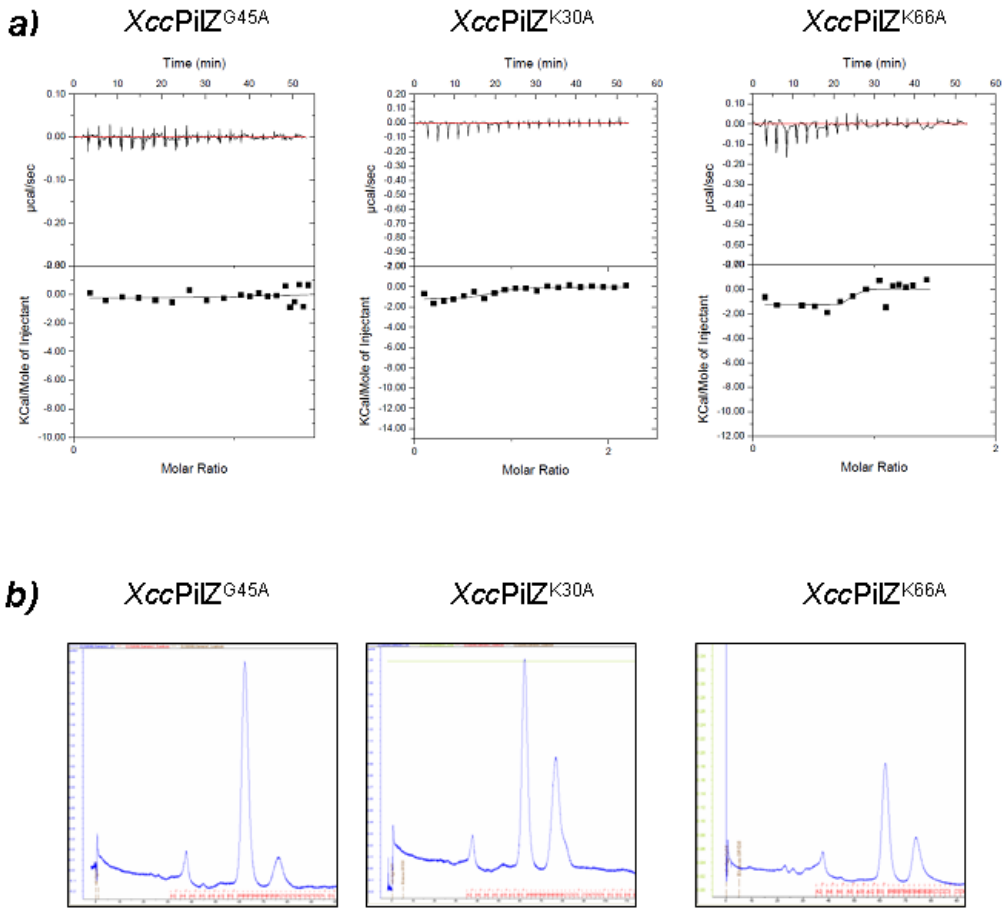

Supplementary Figure S3. a) ITC titrations of the with the *Xcc*PilZ$_{1028}$ variants. Almost no heat was released when the complex was titrated with the G45A (left), K30A (middle), and K66A (right) variants. b) Gel filtration chromatography

(Superdex 75) of the *Xcc*FimX^{EAL}–c-di-GMP complex with the *Xcc*PilZ$_{1028}$ variants. Only small amount of the ternary complex was formed when the *Xcc*FimX^{EAL}–c-di-GMP complex was mixed with the G45A (left), K30A (middle), and K66A (right) variants of the *Xcc*PilZ$_{1028}$ domain.

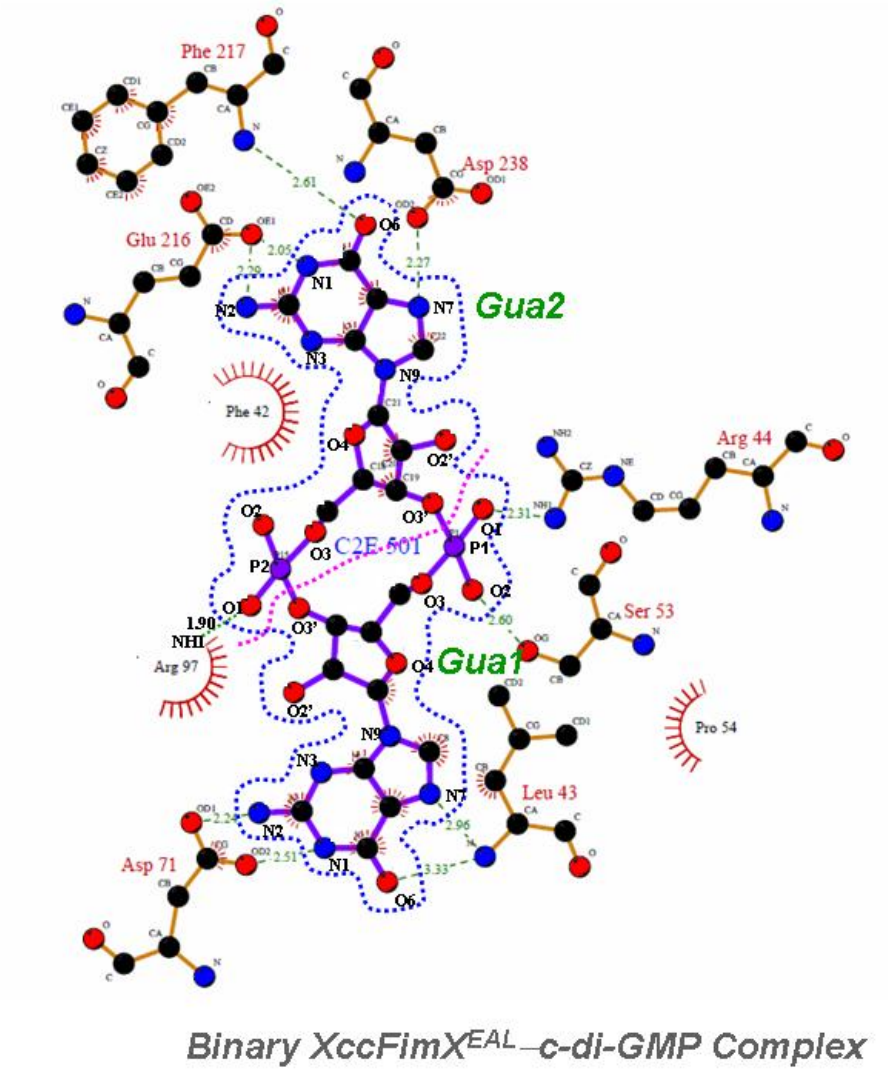

Supplementary Figure S4. LigPlot (Wallace et al., 1995) of the binary *Xcc*FimX^{EAL}–c-di-GMP complex. C-di-GMP is enclosed in blue dotted line, and Gua1 and Gua2 were divided by a pink dotted line.

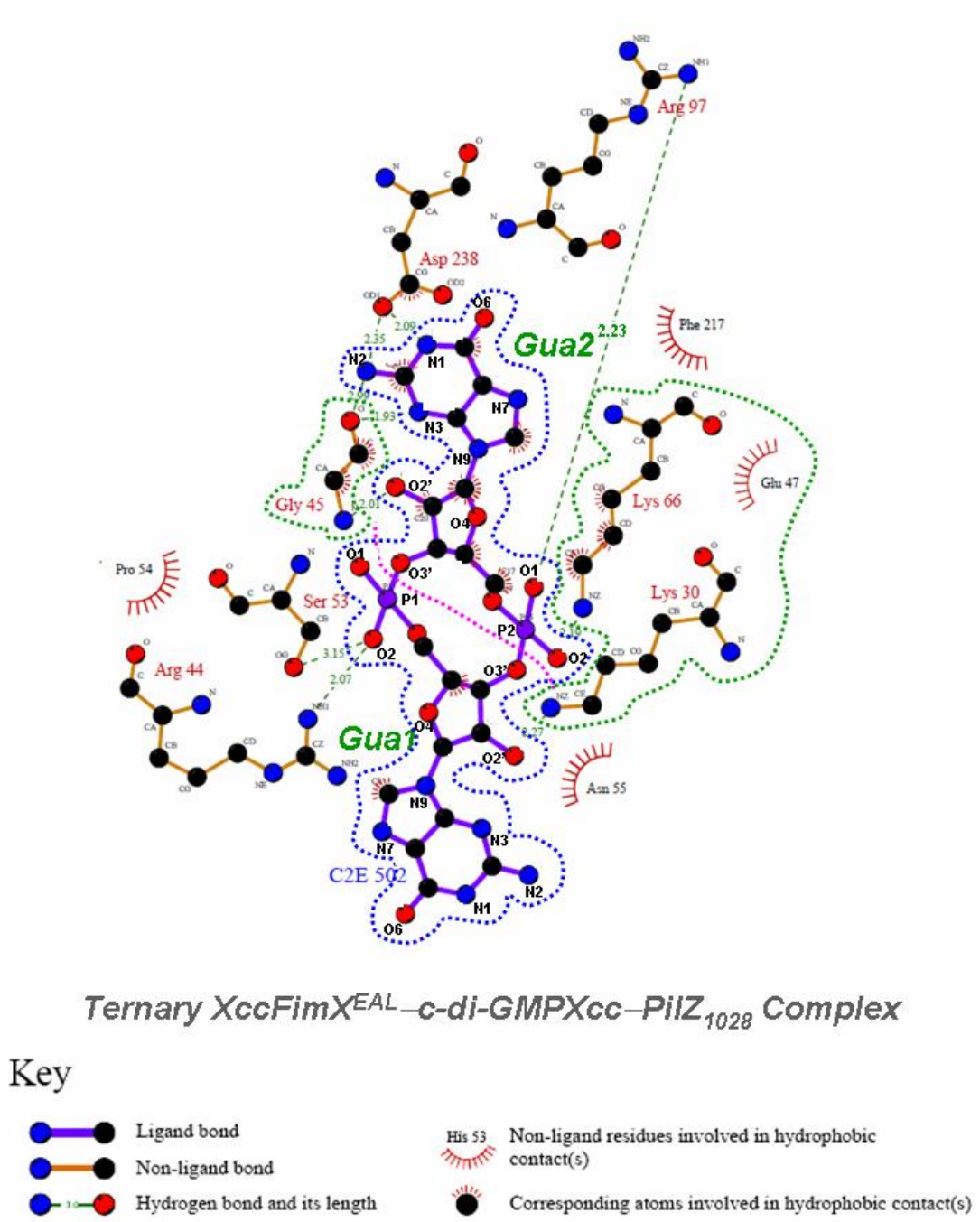

Supplementary Figure S5. LigPlot (Wallace et al., 1995) of the ternary *Xcc*FimX^{EAL}–c-di-GMP–*Xcc*PilZ$_{1028}$ complex. C-di-GMP is enclosed in blue dotted line, and Gua1 and Gua2 were divided by a pink dotted line. The amino acid residues from *Xcc*PilZ$_{1028}$ were enclosed in green dotted line.

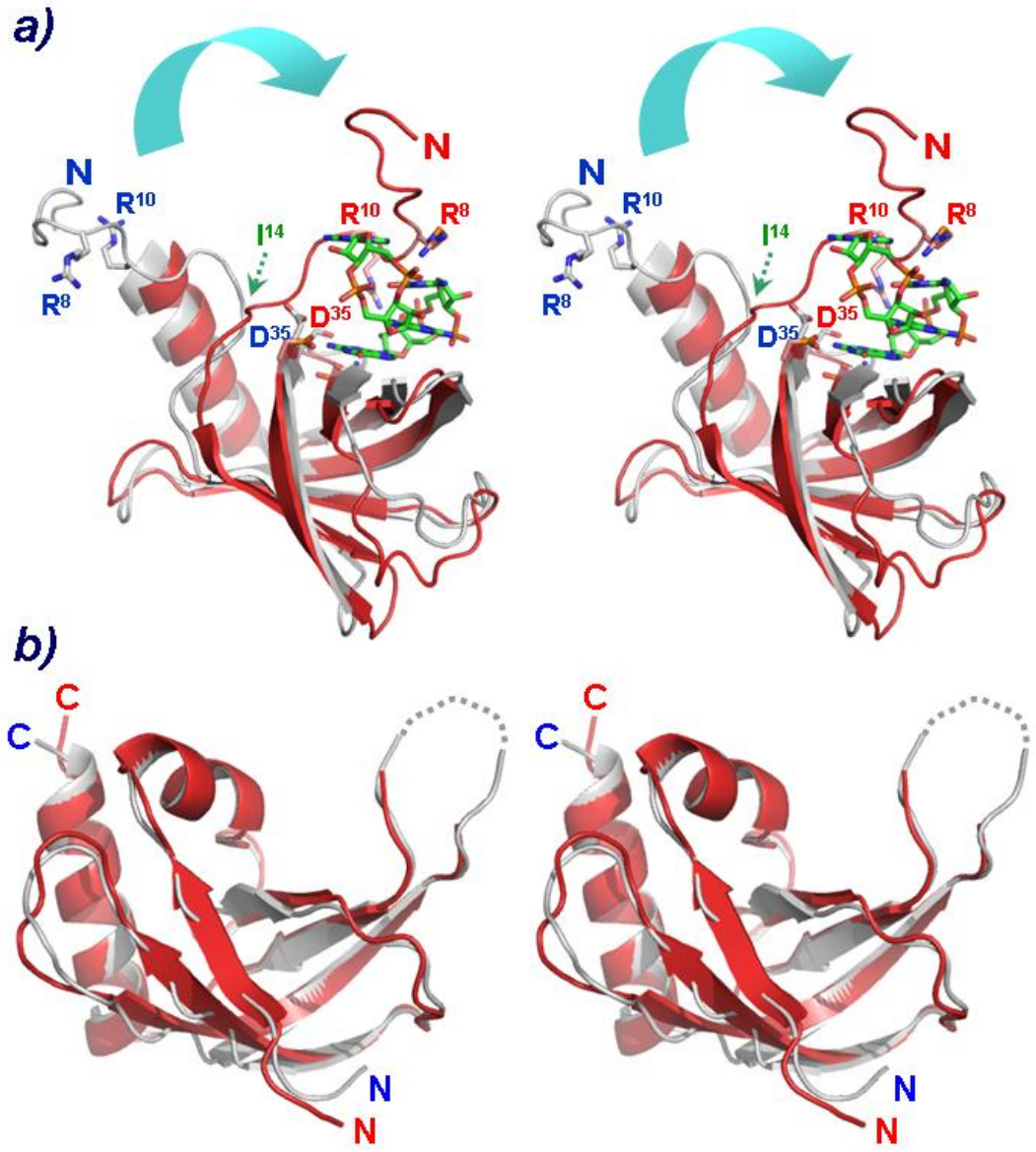

Supplementary Figure S6. a) Superimposition of type I PilZ domain protein PA4608 in its apo- (PDB:1YWU, cartoons colored in gray) and c-di-GMP bound forms (PDB:2L74, cartoons colored in red). A significant flipping of the N-terminal RxxR signature motif at the hinge residue I^{14} is observed when PA4608 binds c-di-GMP (marked by a curved arrow in bluie). Several crucial residues in the signature motif are marked with residue numbers. The carbon atoms of c-di-GM in 2L74 are colored in green. b) Superimposition of type II PilZ domain protein Xcc1028 in its apo-

(PDB:3DSG cartoons colored in red) and $FimX^{EAL}$-c-di-GMP-bound forms (cartoons colored in gray). No major backbone conformational changes are detected.